

# In vivo Biodistribution and Urinary Excretion of Mesoporous Silica Nanoparticles: Effects of Particle Size and PEGylation

Qianjun He, Zhiwen Zhang, Fang Gao, Yaping Li,\* and Jianlin Shi\*

The *in vivo* biodistribution and urinary excretion of spherical mesoporous silica nanoparticles (MSNs) are evaluated by tail-vein injection in ICR mice, and the effects of the particle size and PEGylation are investigated. The results indicate that both MSNs and PEGylated MSNs of different particle sizes (80–360 nm) distribute mainly in the liver and spleen, a minority of them in the lungs, and a few in the kidney and heart. The PEGylated MSNs of smaller particle size escape more easily from capture by liver, spleen, and lung tissues, possess longer blood-circulation lifetime, and are more slowly biodegraded and correspondingly have a lower excreted amount of degradation products in the urine. Neither MSNs nor PEGylated MSNs cause tissue toxicity after 1 month *in vivo*.

## 1. Introduction

In vivo biodistribution, lifetime, and toxicity are vitally important aspects of biosafety, and currently are hot topics of nanomaterial research. The biodistribution profiles of nanomaterials are of essential significance for the investigation of their passive target capacities, tissue/organ toxicity, and biomedical applications.<sup>[1–7]</sup> As for nanomaterials used as drug-delivery vehicles and/or detecting agents, such as mesoporous silica nanoparticles (MSNs), carbon nanotubes (CNTs), liposomes, nanogels, Au nanorods, fluorescent quantum

dots, superparamagnetic nanoparticles, and so on, their biodistribution data can provide important references for the realization of targeted drug delivery and specialized tissue imaging.<sup>[2–8]</sup> When the passive targeting effect of nanomaterials needs to be utilized for drug delivery, nanomaterials would be expected to be selectively captured by the targeted organ. However, nanomaterials should be designed to keep away from geometrical capture and phagocytosis when used to actively target a specific organ. When nanomaterials of no toxicity are to be used for sustained drug release, it would be highly desirable that they were localized in certain positions and kept stable for a considerably long time period.

Owing to their unique mesostructural features (high specific surface area, large pore volume, and tunable pore structure), high drug-loading capacity, and sustained-release profiles, research into applications of MSNs in the biomedicine field has attracted broad attention.<sup>[9–24]</sup> MSNs have been extensively suggested for use in controllable drug delivery,<sup>[9–17]</sup> biosignal probing,<sup>[17,18]</sup> gene transport and expression,<sup>[17–21]</sup> biomarking,<sup>[22]</sup> and many other important biological applications.<sup>[23–25]</sup> Meanwhile, the biological effects of MSNs at different levels, from molecule, cell, and blood to organ/tissue, which involve cytotoxicity,<sup>[26–30]</sup> biodegradability,<sup>[31,32]</sup> blood compatibility,<sup>[29,33,34]</sup> biodistribution, and excretion, are also

Dr. Q. J. He, Prof. J. L. Shi  
State Key Laboratory of High Performance Ceramics and Superfine Microstructure  
Shanghai Institute of Ceramics  
Chinese Academy of Sciences  
1295 Ding-Xi Road, Shanghai 200050, P. R. China  
E-mail: jlshi@sunm.shcnc.ac.cn

Dr. Z. W. Zhang, Dr. F. Gao, Prof. Y. P. Li  
Shanghai Institute of Material Medica  
Chinese Academy of Sciences  
555 Zu Chong-Zhi Road  
Shanghai 201203, P. R. China  
E-mail: ypli@mail.shcnc.ac.cn

DOI: 10.1002/smll.201001459

drawing great attention and have become current hot topics in biosafety research.<sup>[26–35]</sup> Therefore, the investigation of the biodistribution and excretion of MSNs is vitally important and necessary for future potential bioapplications. However, reports on the *in vivo* biodistribution, excretion, and toxicity of MSNs are still very rare. Recently, Mou and co-workers used magnetic resonance imaging (MRI) and fluorescence imaging techniques to investigate the biodistribution of fluorescence/magnetism-functionalized MSNs (Mag-Dye@MSNs) 50–100 nm in diameter, and found that a majority of Mag-Dye@MSNs were located in liver (35.3%) and a minority of them in kidney (9.0%), lung (8.3%), spleen (8.0%), and heart (4.5%) of ICR mouse after eye vein injection for 6 h.<sup>[8,35]</sup> However, the long-term *in vivo* biodistribution, excretion, and tissue compatibility of MSNs of different particle sizes are still unclear to date as far as we know, since the particle size of nanomaterials is generally considered as one of the most important factors determining their biological effects.

In addition to the particle size modulation, surface modification is generally used to change the biodistribution behavior of silica nanomaterials.<sup>[36–38]</sup> Recently, Wang and co-workers found that PEGylation (PEG=polyethylene glycol) was helpful for silica nanomaterials (45 nm) to escape from phagocytosis, which led to increased blood-circulation lifetime, and degradation products of silica nanomaterials could be excreted through the renal system of mouse.<sup>[38]</sup> Very recently, we reported an effective PEGylation strategy for MSNs, and a high hemocompatibility of PEGylated MSNs (PEG-MSNs) was achieved.<sup>[33]</sup>

It is clear that the particle size and surface modification are among the most important aspects affecting the *in vivo* biodistribution and toxicity of MSNs. Herein, the biodistribution and excretion of MSNs of different particle sizes (80, 120, 200, and 360 nm) are investigated *in vivo* for up to 1 month, and the effect of PEGylation is also studied. In addition, the tissue compatibility of MSNs and PEG-MSNs is also evaluated by histopathological analyses. MSN and PEG-MSN samples 80, 120, 200, and 360 nm in diameter are labeled MSNs-80, MSNs-120, MSNs-200, and MSNs-360, and PEG-MSNs-80, PEG-MSNs-120, PEG-MSNs-200, and PEG-MSNs-360, respectively.

## 2. Results and Discussion

### 2.1. Morphology and Mesostructure of MSNs and PEG-MSNs

**Figure 1** and Figure S1 in the Supporting Information show transmission electron microscopy (TEM) images of PEG-MSNs and MSNs of different particle sizes, respectively. TEM analyses indicate that MSNs-80, MSNs-120, MSNs-200, and MSNs-360 have uniform particle sizes of about 80, 120, 200, and 360 nm, respectively. Both MSNs and PEG-MSNs of various particle sizes have a regular spherical morphology and high dispersivity, and the particle sizes of MSNs show no visible change under TEM imaging after the PEGylation. In addition, both MSNs and PEG-MSNs of various particle sizes show uniform mesoporous channels aligned radially from the center to the outside of the particles. Moreover,

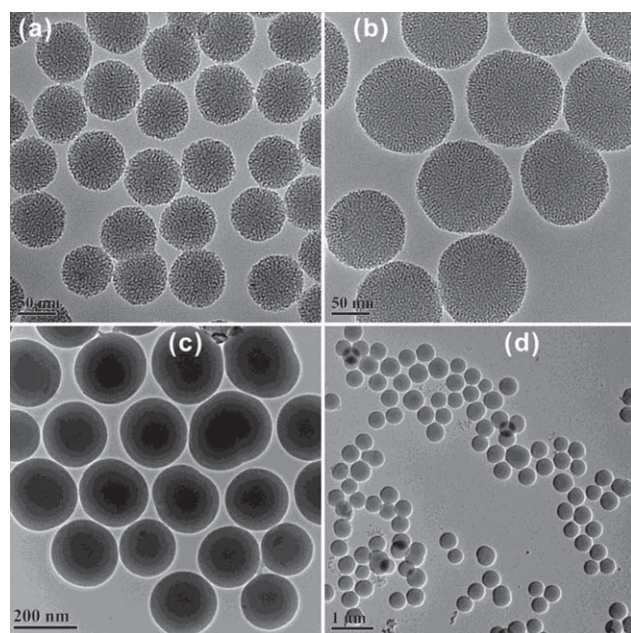


**Figure 1.** TEM images of PEG-MSNs of different particle sizes: PEG-MSNs-80(a), PEG-MSNs-120(b), PEG-MSNs-200(c), and PEG-MSNs-360(d). Scale bars: 50 nm, 50 nm, 200 nm, and 1  $\mu$ m, respectively.

both MSNs and PEG-MSNs of various particle sizes possess partially ordered mesoporous structures, as evidenced from small-angle X-ray diffraction (SAXRD) patterns, and the PEGylation does not have any impact on the ordering of mesoporous structures of MSNs of various particle sizes (**Figure 2** and Figure S2, Supporting Information). In addition,

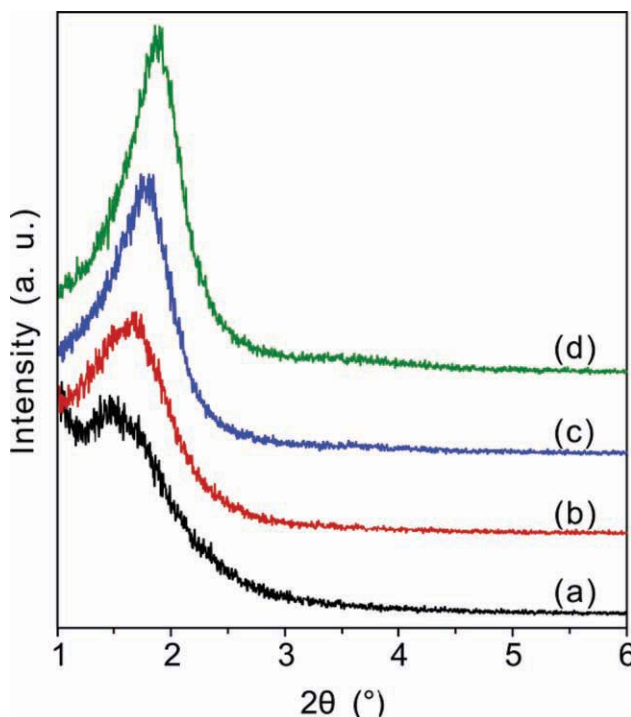


**Figure 2.** SAXRD patterns of PEG-MSNs of different particle sizes: PEG-MSNs-80 (a), PEG-MSNs-120 (b), PEG-MSNs-200 (c), and PEG-MSNs-360 (d).

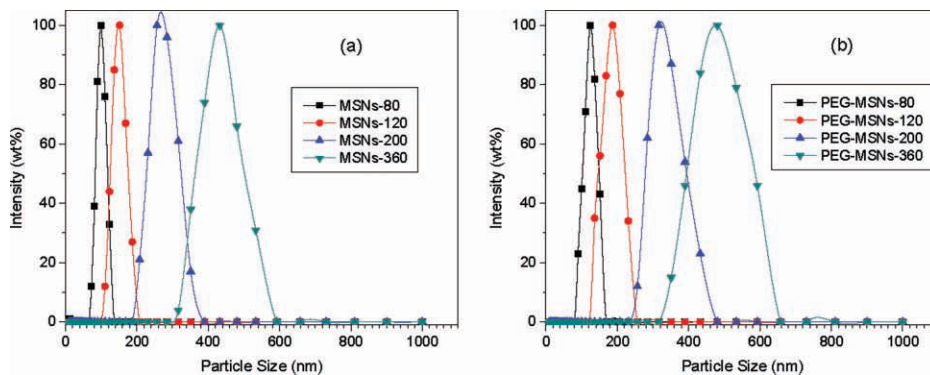


**Figure 3.** Particle size distributions of MSNs (a) and PEG-MSNs (b) of different particle sizes as measured by the DLS technique.

MSNs of larger particle size show a more intensive diffraction peak at  $2\theta = 1.5\text{--}2^\circ$ , which implies a relatively more ordered mesoporous structure. Particle size distributions of various MSN and PEG-MSN samples are measured by dynamic light scattering (DLS; **Figure 3**), which reveals that the hydrodynamic particle sizes of all samples are slightly or a little larger than those resulting from TEM imaging, and the hydrodynamic particle size of PEG-MSNs is larger than that of MSNs of the same particle size. However, the particle size distributions of MSNs and PEG-MSNs, especially MSNs-80 and PEG-MSNs-80, are rather sharp, which suggests that all samples have good dispersivity, regardless of PEGylation.

## 2.2. Biodistribution of MSNs and PEG-MSNs of Different Particle Sizes

The biodistributions of MSNs and PEG-MSNs of size 80, 120, 200, and 360 nm in heart, liver, spleen, lung, and kidney over different time periods of up to 1 month were comparatively investigated by fluorescence intensity measurements (**Figure 4**) and qualitative observation (**Figure 5** and Figure S3, Supporting Information), and the time dependence of their biodistribution was also studied. For qualitative assay, each discretized tissue was cut into slices for directly observing the distribution of green-fluorescent sample particles in tissues under a fluorescence microscope. For quantitative measurements, each discretized tissue was homogenized and extracted for green-fluorescent samples, and then the sample concentrations in tissues were measured by a fluorescence microplate reader. In Figure 5 and Figure S3 in the Supporting Information, the green fluorescence expresses fluorescence-functionalized MSNs, and the fluorescence intensity and coverage area in tissue slices qualitatively reflect the biodistributed amounts of the particles. It could be clearly observed that MSNs and PEG-MSNs of different particle sizes were mainly located in liver and spleen, a minority of them in lung, and a few in kidney and heart, in accordance with the results from Figure 4. Compared with spleen, the overall amounts of the samples in liver were in fact higher although their biodistribution densities were slightly lower, because the weight of a whole liver was about sevenfold higher than that of a whole spleen.

### 2.2.1. Effect of PEGylation

Compared with MSNs, the biodistributions of PEG-MSNs of the same particle sizes in liver, spleen, and lung were visibly lower, as shown by Figure 4, Figure 5, and Figure S3 in the Supporting Information. These results indicated that PEGylation prevented the MSNs from being captured by liver, spleen, and lung tissues to a large extent, especially for MSNs of the relatively large particle size of 360 nm, which could result from the longer blood-circulation lifetime of PEG-MSNs.

In more detail, PEGylation significantly decreased the bio-distributed percentages of PEG-MSNs of different particle sizes in liver and spleen within 30 min of tail intravenous injection, as shown in Figure 4e and f. This suggests that the recognition and phagocytosis of MSNs by liver and spleen phagocytes became much less significant after PEGylation, especially for PEG-MSNs 360 nm in diameter. Compared to the situations in liver and spleen, the PEGylation is especially effective in preventing MSNs from being captured by lung, even within 30 min of injection, for all MSN samples of different sizes. However, it is a little less effective in decreasing the biodistributed percentage for smaller-sized MSNs in such a short time period, as can be seen in Figure S3 in the Supporting Information. This suggests that PEG-MSNs of different particle sizes could escape from recognition and phagocytosis by lung phagocytes and also mechanical interception and capture by the capillary vessel beds of lung, and therefore the biodistributions in lung were depressed by suitable PEGylation.

### 2.2.2. Effect of Particle Size

The biodistributed percentages of both MSNs and PEG-MSNs in liver and spleen increased, on the whole, with an increase of the particle sizes for a short time period of 30 min, with the exception of PEG-MSNs of diameter 360 nm in spleen, as shown in Figure 4e and f. This shows that both MSNs and PEG-MSNs of larger particle size can be more easily captured by the organs, while PEGylation of 360-nm MSNs is extraordinarily effective in preventing the particles being captured in spleen within 30 min of injection.

### 2.2.3. Biodistribution Change with Post-injection Time

The biodistribution of MSNs was ever changing with time after injection, and was also dependent on the particle size of

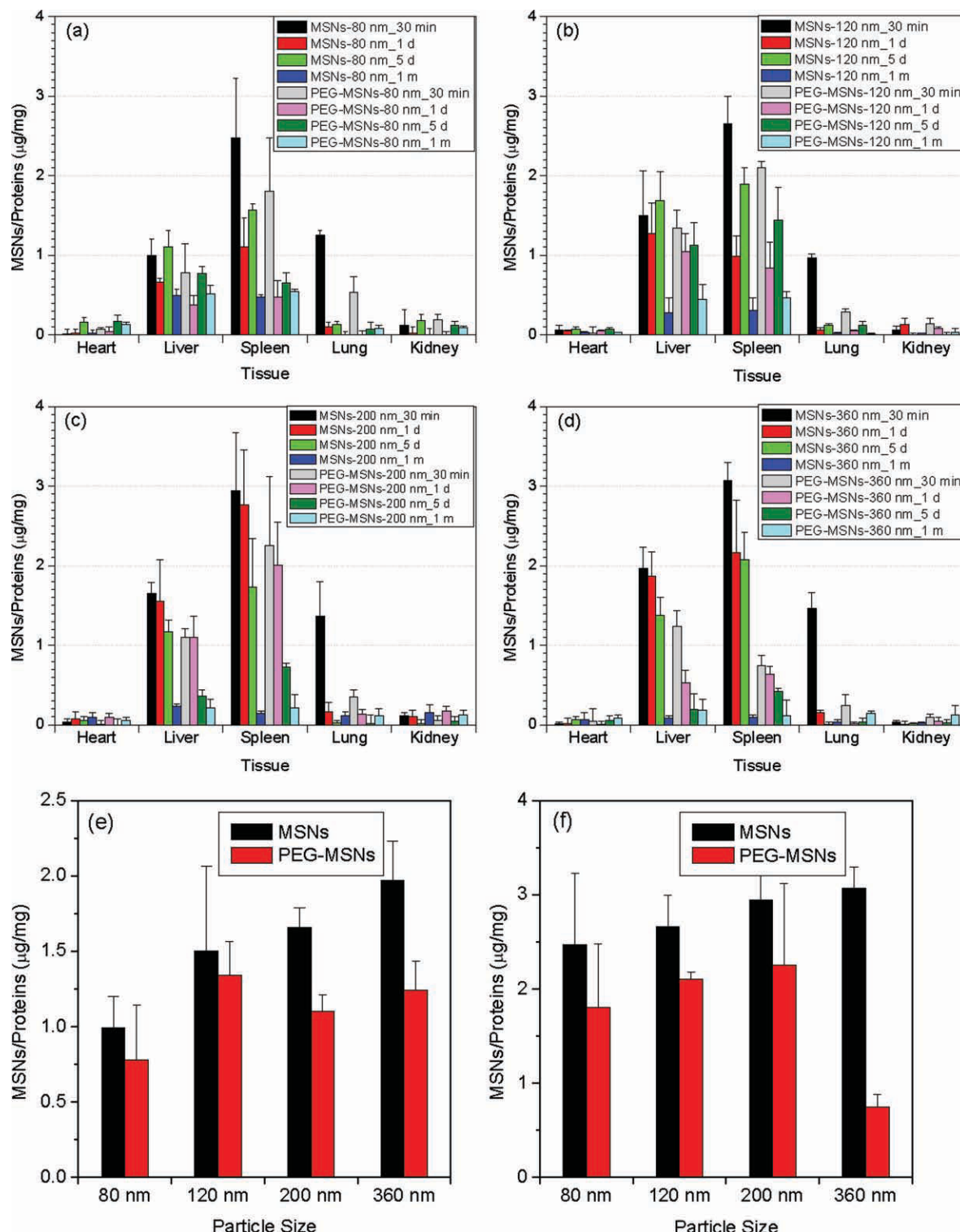


**Figure 4.** Biodistribution percentages of MSNs and PEG-MSNs of particle sizes 80 (a), 120 (b), 200 (c), and 360 nm (d) in heart, liver, spleen, lung, and kidney of ICR mice after tail intravenous injection at different time periods of 30 min, 1 day, 5 days, and 1 month, and comparisons of the biodistribution of MSNs and PEG-MSNs of different particle sizes in liver (e) and spleen (f) of ICR mice 30 min after tail intravenous injection.

the MSNs and was influenced by the PEGylation. This was probably correlated to the different capture features of various organs and the in vivo degradation behavior of MSNs.

For MSNs-80, PEG-MSNs-80, MSNs-120, and PEG-MSNs-120, the biodistributed percentages of these samples

in liver and spleen decreased generally, then increased, and finally decreased again with time post-injection, as shown in Figure 4a and b. Initially, the biodistributed concentration decreasing process in a short time period of 1 day can most likely be attributed to the fast degradation of PEG-MSNs

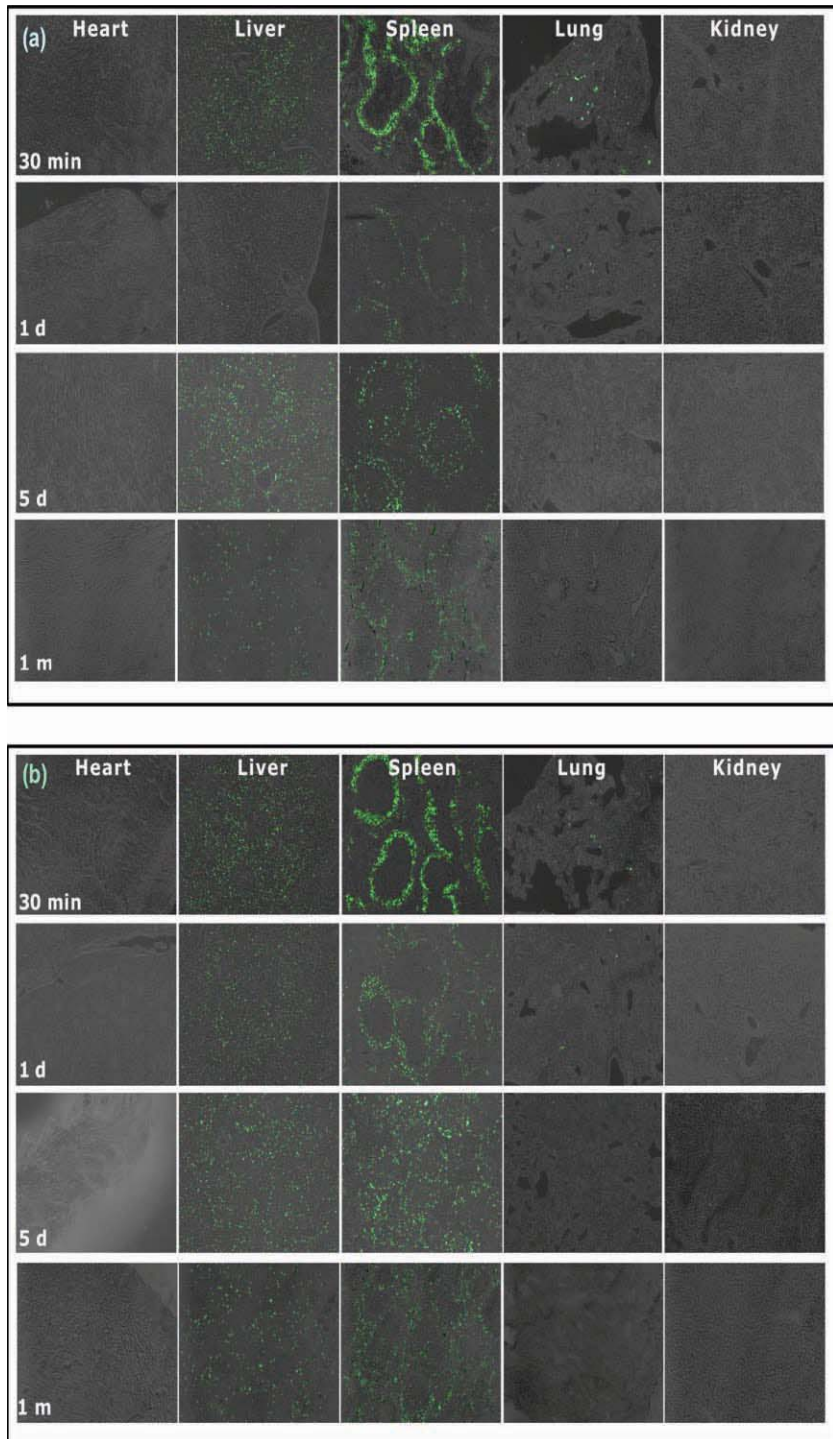


**Figure 5.** Fluorescence images of heart, liver, spleen, lung, and kidney tissue slices from ICR mice injected with MSNs (a) and PEG-MSNs (b) 80 nm in diameter at different time periods (30 min, 1 day, 5 days, and 1 month). Images of MSNs and PEG-MSNs of size 120, 200, and 360 nm are provided in the Supporting Information (Figure S3).

and MSNs, as recently discovered by us in the case of in vitro simulation.<sup>[32]</sup> However, within 5 days of injection, the re-increase of the biodistributed percentages in liver and spleen could be caused by the continuous capture and decreased degradation rates of PEG-MSNs and MSNs,

MSNs-360 but relatively more MSNs-80, PEG-MSNs-80, MSNs-120, and PEG-MSNs-120 staying in liver and spleen 1 month after injection (Figure S3), mainly owing to the relatively slow but continued capture and biodegradation of smaller MSNs by the tissues.

probably resulting in their continuous accumulation and increase of the local concentration. This can be understood by the in vitro simulated experimental results indicating that the degradation process of MSNs can be severely suppressed by increasing the MSN concentration.<sup>[32]</sup> This also implies that there were always both uncaptured PEG-MSNs and MSNs remaining and circulating in the blood. Moreover, compared with MSNs, more PEG-MSNs of the same particle sizes were not captured by liver and spleen, thus implying that PEG-MSNs have a longer blood-circulation lifetime. Within 1 month of injection, the biodistributed percentages of PEG-MSNs and MSNs in liver and spleen decreased again as compared with the case of the fifth day, which should be due to their slow but continued degradation.<sup>[32]</sup> In addition, it was found that most PEG-MSNs and MSNs were degraded according to their decreased biodistributed concentrations (Figure 5 and Figure S3) and contents (Figure 4a and b), and could be degraded completely in the prolonged time period. Interestingly, the concentration decrease of MSNs in lung from 30 min to 1 day post-injection was especially remarkable. Furthermore, neither MSNs nor PEG-MSNs of different particle sizes were found distributed at significant levels in lung (Figure 4 and Figure S3) at and beyond 1 day of injection, which might be due to their biodegradation and/or transfer to other tissues under a high hemoperfusion rate of  $\approx 4.5 \text{ L min}^{-1}$ .

For MSNs-200, PEG-MSNs-200, MSNs-360, and PEG-MSNs-360 of relatively larger particle sizes, the biodistributed percentages of PEG-MSNs and MSNs in liver and spleen kept decreasing with time post-injection within the time period of 30 min to 1 month (Figure 4c and d, and Figure S3), probably because a great majority of these nanoparticles had been captured by liver and spleen in the first 30 min (or longer time) after injection, and thus their degradation rates were higher than their accumulation rates beyond 30 min post-injection. Therefore, there were very few MSNs-200, PEG-MSNs-200, MSNs-360, and PEG-

### 2.3. Blood Clearance of MSNs and PEG-MSNs of Different Particle Sizes

The main aim of the PEGylation is to help MSNs to escape from phagocytosis and capture by various organs and thus possess an increased blood-circulation lifetime. **Figure 6** shows the pharmacokinetic processes and mean residence time (MRT) of various MSN and PEG-MSN samples with different particle sizes in rat blood. It was found that PEG-MSNs are cleared from blood more slowly than MSNs of the same particle sizes (Figure 6c), probably due to the shielding effect of PEGylation. For both MSNs and PEG-MSNs, nanoparticles of smaller sizes have a longer blood-circulation lifetime (Figure 6c), which possibly results from the slower capture by various organs such as liver and spleen, as aforementioned. Therefore, the PEGylation and the particle size are two important factors impacting the blood-circulation lifetime of MSNs. The PEG-MSNs-80 sample with the smallest particle size (80 nm) possesses the longest blood-circulation lifetime in the present investigation, and there is still about 20 µg PEG-MSNs per gram blood 1 h after injection. Because of their relatively longer residence in blood, the PEG-MSNs of small particle size should have more potential therapeutic applications, particularly for cancer therapy.

### 2.4. Urinary Excretion of Degraded MSNs and PEG-MSNs of Different Particle Sizes

Wang and co-workers discovered that both PEGylated and non-PEGylated silica nanoparticles could be partly excreted through the renal excretion route, by a qualitative determination of the fluorescence signal in urine of intravenously injected mice.<sup>[38]</sup> Similarly in this work, we tried to confirm whether MSNs and PEG-MSNs of different particle sizes can also be excreted through the urinary system of mice, since MSNs are also intravenously injected through the tail vein and captured mainly by liver and spleen, as mentioned above. **Figure 7** shows the concentrations of degraded MSNs and PEG-MSNs of different particle sizes in the urine of ICR mice at different time points, which reflect the *in vivo* mean degradation rates and the excretion amount of degradation products in different time periods of up to 1 month after tail intravenous injection. At 30 min post-injection, a number of silica degradation products were excreted from urine, and their excreted quantities remarkably increased with the increase of particle size of MSNs (or PEG-MSNs); the excreted quantities of degradation products of PEG-MSNs were distinctly less than those of MSNs of the same particle sizes. It is thought that MSNs of larger particle sizes were more easily and mostly captured by liver and spleen in 30 min, as indicated by the above discussion, which led to their faster biodegradation and consequently the larger excreted quantities of their degradation products. The PEGylation apparently hindered the capture by liver and spleen, which resulted in the slower biodegradation of PEG-MSNs and consequently lower excreted quantities of their degradation products as compared with MSNs of the same particle sizes.

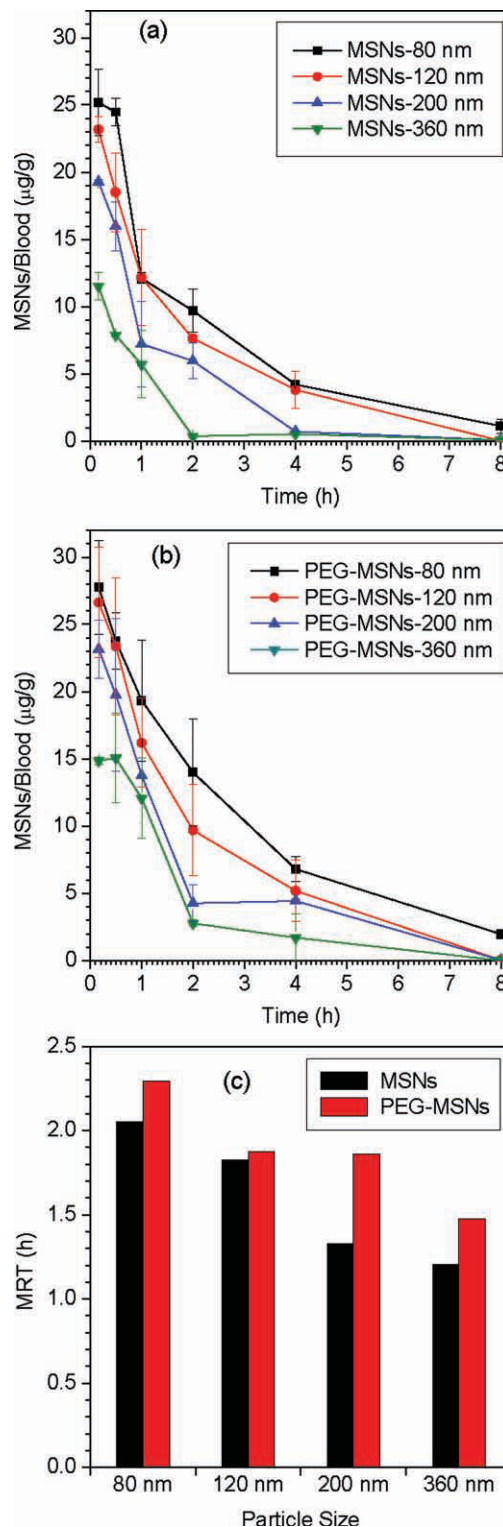


**Figure 6.** Pharmacokinetic processes of MSNs (a) and PEG-MSNs (b) of different particle sizes (80, 120, 200, and 360 nm) in blood of Sprague-Dawley rats, and the particle size dependence of MRT (c).

As expected, the excreted quantities of the degradation products of both MSNs and PEG-MSNs of different particle sizes decreased with time. However, the excreted quantities of the degradation products of MSNs and PEG-MSNs of relatively larger particle sizes (200 and 360 nm) decreased more

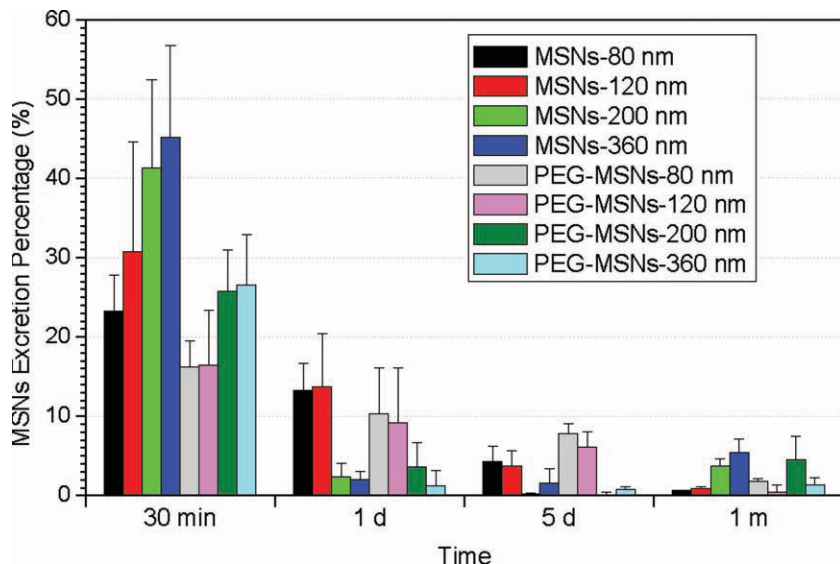


**Figure 7.** Excretion percentages of the degradation products of MSNs and PEG-MSNs of different particle sizes (80, 120, 200, and 360 nm) in urine of ICR mice up to 1 month after tail intravenous injection.

remarkably within 30 min to 1 day after injection. As mentioned above, a majority of MSNs of larger particle sizes were captured mainly by liver and spleen in a short time of 30 min after injection, which caused the continuously decreased biodistribution percentages beyond 30 min; therefore, both their degradation amounts and corresponding excreted quantities of degradation products decreased at faster rates. Comparatively, however, the degradation amounts and corresponding excreted quantities of the degradation products of PEG-MSNs of relatively small particle size decreased more slowly, owing to their longer blood-circulation lifetime. Nevertheless, the overall excreted quantities of the degradation products of all MSN and PEG-MSN samples of various particle sizes beyond 30 min after intravenous injection were much lower than those within 30 min, in agreement with the lower biodistributed concentration in the tissues, thus indicating that the MSNs in this study were indeed degradable *in vivo*.

It is noticeable that the urinary excretion percentage can reach almost 15–45% of the total injected amount of MSNs for the investigated samples at only 30 min post-injection, and was especially high (up to 45.2%) for the MSNs-360 sample. The total urinary excretion at these four discontinuous time points (30 min, 1 day, 5 days, 1 month) reaches 54.2% for the MSNs-360 sample, with the initial 30 min being the main period of renal clearance of the MSNs. Therefore, we can conclude that excretion through urine should be by one of two main approaches, that is, renal clearance or hepatobiliary clearance. Unfortunately, according to the present data, the exact total excretion percentages of MSNs and/or the degradation products via urinary clearance or hepatobiliary clearance is still unknown.

## 2.5. Histopathological Evaluation of MSNs and PEG-MSNs of Different Particle Sizes

After injection with MSNs and PEG-MSNs of various particle sizes for 1 month, all treated ICR mice survived, and

no abnormal behavior or symptoms were visually observed. Neither erythema nor edema was visible at the injection sites. This suggests that both MSNs and PEG-MSNs caused no irreparable impairment of the vessel wall and the endothelial cell structure. No abnormality was noted in the gross examination of tissues.

**Figure 8** shows fluorescence microscopy images of tissue slices from ICR mice injected with MSNs and PEG-MSNs of various particle sizes after 1 month. Compared with the blank control, all tissues (heart, liver, spleen, lung, and kidney) showed no acute pathological change in the microscopic examination, which indicated that neither MSNs nor PEG-MSNs caused significant tissue toxicity and inflammation during 1 month *in vivo*; therefore, both MSNs and PEG-MSNs possessed good tissue compatibility. Such a compatibility can be attributed to the

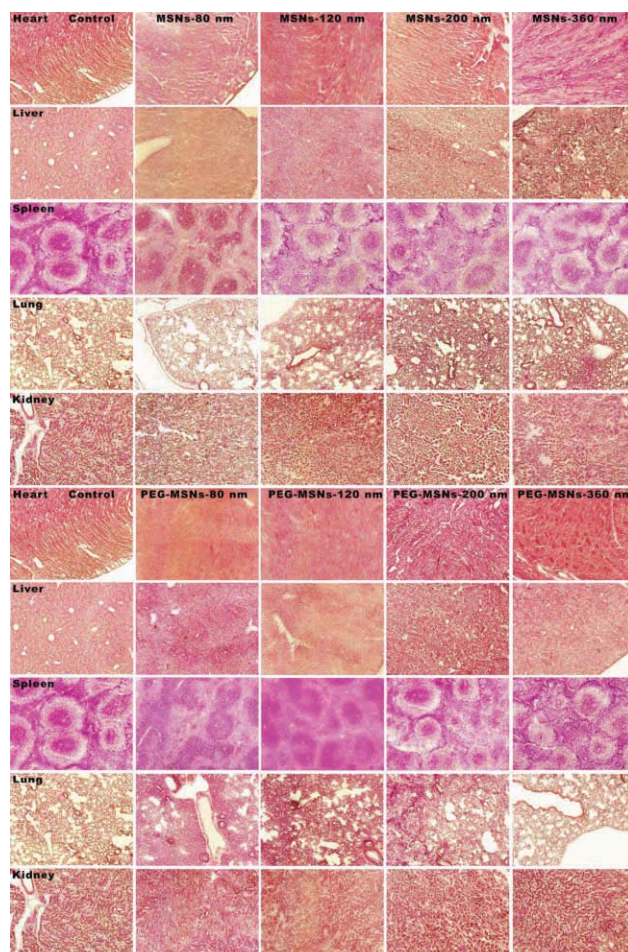


**Figure 8.** Histological examination of tissues (heart, liver, spleen, lung, and kidney) from ICR mice injected with MSNs and PEG-MSNs of different particle sizes (80, 120, 200, and 360 nm) through tail intravenous injection after 1 month.

stable physicochemical properties, biodegradability, and biocompatibility of the particles and biodegradation products.

### 3. Conclusion

The biodistribution and excretion of MSNs and PEG-MSNs of different particle sizes (80, 120, 200, and 360 nm) have been investigated with ICR mice via tail-vein injection. MSNs and PEG-MSNs of different particle sizes were mainly located in liver and spleen, a minority of them in lung, and a few in kidney and heart. According to the balance between capture and biodegradation, the biodistribution percentages of MSNs and PEG-MSNs of the relatively smaller particle sizes of 80 and 120 nm in liver and spleen firstly decreased, then increased, and finally decreased again; however, those of relatively larger particle sizes of 200 and 360 nm decreased continuously in the time period from 30 min to 1 month after injection. The PEGylation of MSNs was effective in partially preventing MSNs from being captured by liver, spleen, and lung, which resulted in lower captured biodistribution concentrations, longer blood-circulation lifetime, slower biodegradation, and correspondingly lower excreted amount of degradation products of PEG-MSNs than MSNs of the same particle sizes. For all the investigated MSNs and PEG-MSNs, the excreted amount of degradation products decreased with time. MSNs of smaller particle sizes could escape more easily from capture by liver and spleen tissues, and were more slowly biodegraded and correspondingly had a lower excreted amount of degradation products. All the treated ICR mice survived well for 1 month after being injected with all MSN and PEG-MSN samples, and no pathological abnormality was observed in both gross and microscopic histological examinations.

### 4. Experimental Section

**Synthesis of MSNs of Different Particle Sizes:** Monodisperse spherical MSNs of controlled particle size were prepared by using cationic–nonionic composite surfactants as the structure-directing agent under neutral conditions, as described in our previous reports.<sup>[26,39]</sup> Initially, appropriate amounts of cetyltrimethylammonium bromide (CTAB) and Brij-56 were completely dissolved in turn in phosphate-buffered saline (PBS, 500 mL, pH 7; 3.43 g KH<sub>2</sub>PO<sub>4</sub> and 0.58 g NaOH) at 95 °C under vigorous stirring, and then tetraethyl orthosilicate (TEOS; 9 mL) was added dropwise. The particle size of the MSNs was well controlled by adjusting the surfactant concentrations and molar ratios of CTAB and Brij-56. After continuous stirring for 8 h, the as-synthesized milk-white precipitates were collected by centrifugation and then washed several times with ethanol. To remove surfactants completely, the as-synthesized materials were refluxed in a mixed solution of ethanol (250 mL) and hydrochloric acid (36–38%, 2 mL) at 80 °C for 6 h, and then centrifuged and washed several times with ethanol. The same reflux operation was repeated several times. The final products were dried for 12 h at 120 °C in a vacuum, and spherical MSNs of different particle sizes (80, 120, 200, and 360 nm) were obtained.

**PEGylation and Fluorescence Functionalization of MSNs of Different Particle Sizes:** The covalent PEGylation of MSNs was carried out with PEG (10 000 Da, Fluka, Neu-Ulm, Germany) at a grafting content of 0.75% for optimal blood compatibility, as described in our previous report.<sup>[33]</sup> Firstly, a silane coupling agent with side-chained PEG (PEG–silane) was synthesized by a hydrogen-transfer nucleophilic addition reaction between the end hydroxyl group of PEG and the isocyanate group of 3-(triethoxysilyl)propyl isocyanate (TESPIC). The adsorbed water in PEG was extracted at 90 °C for 3 h in a vacuum. Then, dried PEG (0.02 mol) was completely dissolved in dry pyridine (80 mL) at 70 °C under continuous stirring and protection by an argon atmosphere in a glove box. After continuous stirring for 6 h, TESPIC (0.02 mol) was added to the above mixed solution. After 24 h, the solvent was removed by vacuum extraction. The residual raw product was washed three times with hexane (80 mL), and then purified by recrystallization in ethanol (40 mL) at 0 °C. The product was isolated by filtration with a Büchner funnel at 0 °C and then dried for 6 h at room temperature in a vacuum. A white waxy PEG–silane was obtained. In addition, a silane coupling agent with side-chain fluorescent groups was also synthesized by a hydrogen-transfer nucleophilic addition reaction between fluorescein isothiocyanate (FITC) and 3-aminopropyltriethoxysilane (APTES) at a molar ratio of 1:1 in ethanol under light-sealed conditions.

MSNs were dispersed in dried toluene, and the mixture was heated at reflux for 24 h at 120 °C. Then the MSN suspension was cooled to room temperature under the protection of a dried argon atmosphere. The ethanol solution of PEG–silane was added dropwise under vigorous stirring, and the mixed solution was heated slowly until boiling. After vigorous stirring for 12 h, the ethanol solution of FITC-APTES was also added dropwise. After another 12 h, the final product was collected by centrifugation, washed with ethanol several times until the complete removal of free fluorescent molecules, and finally dried overnight at 100 °C in a vacuum. Both covalently PEGylated and FITC-functionalized MSNs of particle sizes 80, 120, 200, and 360 nm were obtained and denoted PEG-MSNs-80, PEG-MSNs-120, PEG-MSNs-200, and PEG-MSNs-360, respectively. In addition, FITC-functionalized MSNs of particle sizes 80, 120, 200, and 360 nm were obtained by following the same procedures without the addition of PEG–silane, and denoted MSNs-80, MSNs-120, MSNs-200, and MSNs-360, respectively.

**Characterization of MSNs and PEG-MSNs of Different Particle Sizes:** The mesostructures of MSNs and PEG-MSNs were characterized by TEM and SAXRD on a JEM-2010 electron microscope at an accelerating voltage of 200 kV and a JSM-6700F electron microscope, respectively. The mean particle size was calculated from the diameters of 50 particles observed in a TEM image. Only parts of the TEM images are shown in Figure 1; however, the particle sizes were measured over the entire TEM images. SAXRD data were recorded on a Rigaku D/Max-2550V diffractometer using CuK $\alpha$  radiation (40 kV and 40 mA) at a scanning rate of 0.4° min<sup>-1</sup> over the range of 1–6° with a step width of 0.002°. The particle size distribution data were collected by DLS in a Mastersizer 2000 analyzer (Malvern Instruments Ltd., UK).

**Animal and Reagent Preparation:** Male ICR mice (20–25 g) and Sprague–Dawley rats (200–250 g) purchased from Sino-British Sippr/BK Lab Animal Ltd. (Shanghai, China) were used for biodistribution evaluation and blood clearance monitoring, respectively. All

animals were monitored and maintained daily under a 12 h light/dark cycle at the Animal Care Facility, and fresh distilled water and food for all animals were available ad libitum. Animals were acclimatized for at least 5 days prior to the experiments. The in vivo experiments were carried out under the guidelines approved by the International Animal Care and Use Committee (IACUC) of Shanghai Institute of Materia Medica, Chinese Academy of Sciences.

A digest solution of NaOH (1 mol L<sup>-1</sup>) and 1% Triton X-100 was prepared and stored at 4 °C. Eight samples (PEG-MSNs-80, PEG-MSNs-120, PEG-MSNs-200, PEG-MSNs-360, MSNs-80, MSNs-120, MSNs-200, and MSNs-360) were ultrasonically dispersed in sterile physiological saline solutions (0.9%) at the same concentration of 4 mg mL<sup>-1</sup>, and these sample solutions were stored at 4 °C under light-sealed conditions.

The protein content of each tissue (expressed by  $C_p$ ) was measured by the bicinchoninic acid (BCA) method using a BCA Protein Assay Kit (Pierce). The BCA solution was prepared by mixing solutions A and B together, and stored at room temperature. The standard curve for protein quantification was plotted and linearly fitted to  $A = 1.3296 \times C - 0.1952$ , wherein  $A$  and  $C$  represent the absorbance (at 560 nm) and concentration of the sample solution, respectively.

**Biodistribution Investigation:** 96 ICR mice were randomly divided into eight groups ( $n = 12$ ), which were intravenously injected through the tail vein with eight solution samples (PEG-MSNs-80, PEG-MSNs-120, PEG-MSNs-200, PEG-MSNs-360, MSNs-80, MSNs-120, MSNs-200, and MSNs-360) at the same dosage of 5 µL g<sup>-1</sup>. The treated mice were maintained under the same experimental conditions and kept surviving for 1 month, and no abnormal behavior or symptoms were visually observed. At several fixed time points (30 min, 1 day, 5 days, 1 month), some mice were sacrificed via cervical dislocation which was followed by the collection of urine. The tissues and organs, such as heart, liver, spleen, lung, and kidney, were discretized, rinsed with sterile physiological saline, and then blotted dry with filter paper. All the discretized tissues were cut into slices 5 µm in thickness followed by polyoxymethylene fixing and paraffin embedding for directly observing the distribution of green-fluorescent sample particles on an Olympus BX51 fluorescence microscope. In the fluorescence assay, all experiments were carried out under light-sealed conditions to avoid FITC photobleaching as far as possible.

Furthermore, a piece of each tissue (50 mg) was homogenized in the above digest solution (3 mL). Cool methanol (200 µL, chromatographic grade) was vortex-mixed with cool tissue homogenate (200 µL) to precipitate most of the proteins in the homogenates and avoid the disturbance of tissue autofluorescence. After 30 min of static processing under light-sealed, cool, and closed conditions, the coagulated protein was removed by centrifugation (20 000 rpm, 8 min) at 4 °C, and then the upper clear solution (200 µL) was added to a black 96-well microplate. The fluorescence data (emission wavelength at 520 nm, excitation wavelength at 480 nm), which indicated the fluorescence intensity of tissue homogenates (expressed by  $A_t$ ), were collected on a TECAN infinite F200 microplate reader. After that, each solution (20 µL) was transferred to another 96-well microplate, and BCA solution (200 µL) was added to each well. After 30 min of static incubation at 37 °C, the absorbance of the solutions at 560 nm was collected on the TECAN infinite F200 microplate reader. Finally, the protein concentrations of tissue homogenates ( $C_{p\_tissue}$ ) were calculated according

to the standard curve function. According to the fluorescence intensity (at 520 nm) and protein concentrations of tissue homogenates, the fluorescence density of samples (expressed by  $A_{s\_tissue}$  in count per mg proteins) in each tissue could be calculated by dividing the fluorescence intensity of tissue homogenates ( $A_t$ , in count per mg tissue) by the protein concentration of tissue homogenates ( $C_{p\_tissue}$ , in mg proteins per mg tissue), namely  $A_{s\_tissue} = A_t / C_{p\_tissue}$ .

To exactly determine the concentrations of fluorescent samples in each tissue, the fluorescence intensity of each unit mass sample in aqueous solution was measured. The sample solution (20 µL, 5 µL g<sup>-1</sup>) was completely dissolved in the digest solution (5 mL). Then each solution (100 µL) and cool methanol (200 µL, chromatographic grade) were vortex-mixed for 2 min. The mixed solution (200 µL) was added to the black 96-well microplate and the fluorescence data (emission wavelength at 520 nm, excitation wavelength at 480 nm) were collected on a TECAN infinite F200 microplate reader. Finally, the fluorescence intensity of each unit mass sample in solution (expressed by  $A_{s0}$ , in count per µg MSNs or per µg PEG-MSNs) could be calculated. Furthermore, the concentration of MSNs in each tissue (expressed by  $C_{s\_tissue}$ , in µg MSNs per mg proteins or µg PEG-MSNs per mg proteins) could be calculated according to the fluorescence density of MSNs ( $A_{s\_tissue}$ , in count per mg proteins) in each tissue and that of each unit mass sample ( $A_{s0}$ , in count per µg MSNs or per µg PEG-MSNs), namely  $C_{s\_tissue} = A_{s\_tissue} / A_{s0}$ .

**Monitoring of Blood Clearance:** Sprague-Dawley rats were randomly divided into eight groups ( $n = 3$ ), which were intravenously injected through the tail vein with eight solution samples (PEG-MSNs-80, PEG-MSNs-120, PEG-MSNs-200, PEG-MSNs-360, MSNs-80, MSNs-120, MSNs-200, and MSNs-360) at the same dosage. The treated rats were maintained under the same experimental conditions. Blood samples were collected at predetermined time points (0, 10 min, 30 min, 1 h, 2 h, 4 h, and 8 h) into tubes with deionized water (3 mL) for complete hemolysis under light-sealed conditions. The collected samples were accurately weighed, centrifuged (20 000 rpm, 8 min) at 4 °C, and washed several times with deionized water. The upper clear solution was discarded, and then the separated MSNs and PEG-MSNs were dissolved in NaOH solution (100 µL, 1 M) and cool methanol (200 µL, chromatographic grade). After 30 min of static processing under light-sealed, cool, and closed conditions, the coagulated protein was removed by centrifugation (10 000 rpm, 10 min) at 4 °C. The upper clear solution (100 µL) was added to the black 96-well microplate and the fluorescence data (emission wavelength at 520 nm, excitation wavelength at 480 nm) were collected on a TECAN infinite F200 microplate reader, which indicated the fluorescence intensity of MSNs in blood ( $A_{s\_blood}$ ). Finally, the concentrations of MSNs in blood ( $C_{s\_blood}$ , in µg MSNs per gram blood or µg PEG-MSNs per gram blood) could be calculated according to the fluorescence intensity of MSN samples in blood ( $A_{s\_blood}$ , in count per gram blood) and that of each unit mass sample ( $A_{s0}$ , in count per µg MSNs or per µg PEG-MSNs), namely  $C_{s\_blood} = A_{s\_blood} / A_{s0}$ .

**Urinary Excretion Investigation:** By the same analysis procedures as those for the fluorescence intensity and protein concentrations of tissue homogenates, liquid urine (5 µL) was mixed with cool methanol (495 µL) and the mixed solutions were used for the determination of the fluorescence intensity ( $A_u$ , in count per mg urine) and protein concentration of urine ( $C_{p\_urine}$ , in mg protein per mg urine). Furthermore, the sample percentages in each

urine specimen ( $P_{s\_urine}$ , in%) could be calculated according to the volume of urine ( $V_{urine}$ , in mL), the protein concentration in urine ( $C_{p2\_urine}$ , in mg protein per mL urine), the fluorescence density of each sample in urine ( $A_{s\_urine} = A_u / C_{p\_urine}$ , in count per mg protein), and the fluorescence intensity of each unit mass sample ( $A_{s0}$ , in count per  $\mu\text{g}$  MSNs or per  $\mu\text{g}$  PEG-MSNs), namely  $P_{s\_urine} = C_{p2\_urine} \times V_{urine} \times A_{s\_urine} / A_{s0}$ .

**Histopathological Evaluation:** Some slices of each tissue, including heart, liver, spleen, lung, and kidney, were stained by the routine hematoxylin-eosin staining method, and then were photographed on an Olympus X51 fluorescence microscope for the histopathology assay.

**Statistical Analysis:** Each experiment was repeated three times, and the results were presented as the mean  $\pm$  standard deviation. The statistical evaluation of data was performed using a two-tailed unpaired Student's *t*-test. A *p*-value of less than 0.05 was considered statistically significant.

## Supporting Information

Supporting Information is available from the Wiley Online Library or from the author.

## Acknowledgements

Q.J.H. and Z.W.Z contributed equally to this work. We acknowledge financial support from the National Nature Science Foundation of China (Grant Nos. 50823007 and 50972154), the National Basic Research Program of China (Grant Nos. 2010CB934000 and 2009CB930304), the National 863 High-Tech Program (Grant No. 2007AA03Z317), the Science and Technology Commission of Shanghai (Grant No. 10430712800), and CASKJCX Projects (Grant Nos. KJCX2-YW-M02 and KJCX2-YW-210).

- [1] F. E. Escoria, M. R. McDevitt, C. H. Villa, D. A. Scheinberg, *Nano medicine (Lond.)* **2007**, *2*, 805–815.
- [2] S. K. Balasubramanian, J. Jittiwat, J. Manikandan, C. N. Ong, L. E. Yu, W. Y. Ong, *Biomaterials* **2010**, *31*, 2034–2042.
- [3] L. Lacerda, A. Bianco, M. Prato, K. Kostarelos, *Adv. Drug Delivery Rev.* **2006**, *58*, 1460–1470.
- [4] H. S. Choi, B. I. Ipe, P. Misra, J. H. Lee, M. G. Bawendi, J. V. Frangioni, *Nano Lett.* **2009**, *9*, 2354–2359.
- [5] C. Lasagna-Reeves, D. Gonzalez-Romero, M. A. Barria, I. Olmedo, A. Clos, V. M. S. Ramanujam, A. Urayama, L. Vergara, M. J. Kogan, C. Soto, *Biochem. Biophys. Res. Commun.* **2010**, *393*, 649–655.
- [6] E. W. M. Vanetten, W. Vanvianen, R. H. G. Tijhuis, G. Storm, I. A. J. M. Bakkerwoudenberg, *J. Controlled Release* **1995**, *37*, 123–129.
- [7] J. X. Wang, G. Q. Zhou, C. Y. Chen, H. W. Yu, T. C. Wang, Y. M. Ma, G. Jia, Y. X. Gao, B. Li, J. Sun, Y. F. Li, F. Jiao, Y. L. Zhao, Z. F. Chai, *Toxicol. Lett.* **2007**, *168*, 176–185.
- [8] C. H. Lee, S. H. Cheng, Y. J. Wang, Y. C. Chen, N. T. Chen, J. Souris, C. T. Chen, C. Y. Mou, C. S. Yang, L. W. Lo, *Adv. Funct. Mater.* **2009**, *19*, 215–222.
- [9] Q. J. He, J. L. Shi, F. Chen, M. Zhu, L. X. Zhang, *Biomaterials* **2010**, *31*, 3335–3346.
- [10] N. K. Mal, M. Fujiwara, Y. Tanaka, *Nature* **2003**, *421*, 350–353.
- [11] Q. Yang, S. H. Wang, P. W. Fan, L. F. Wang, Y. Di, K. F. Lin, F. S. Xiao, *Chem. Mater.* **2005**, *17*, 5999–6003.
- [12] Y. F. Zhu, J. L. Shi, W. H. Shen, X. P. Dong, J. W. Feng, M. L. Ruan, Y. S. Li, *Angew. Chem. Int. Ed.* **2005**, *44*, 5083–5087.
- [13] T. D. Nguyen, K. C. F. Leung, M. Liong, C. D. Pentecost, J. F. Stoddart, J. I. Zink, *Org. Lett.* **2006**, *8*, 3363–3366.
- [14] S. M. Zhu, Z. Y. Zhou, D. Zhang, *ChemPhysChem* **2007**, *8*, 2478–2483.
- [15] S. Giri, B. G. Trewyn, M. P. Stellmacher, V. S. Y. Lin, *Angew. Chem. Int. Ed.* **2005**, *44*, 5038–5044.
- [16] Y. Z. You, K. K. Kalebaila, S. L. Brock, D. Oupicky, *Chem. Mater.* **2008**, *20*, 3354–3359.
- [17] M. Liong, J. Lu, M. Kovochich, T. Xia, S. G. Ruehm, A. E. Nel, F. Tamanoi, J. I. Zink, *ACS Nano* **2008**, *2*, 889–896.
- [18] I. I. Slowing, B. G. Trewyn, S. Giri, V. S. Y. Lin, *Adv. Funct. Mater.* **2007**, *17*, 1225–1236.
- [19] J. F. Diaz, K. J. Balkus, *J. Mol. Catal. B: Enzym.* **1996**, *2*, 115–126.
- [20] D. R. Radu, C. Y. Lai, K. Jeftinija, E. W. Rowe, S. Jeftinija, V. S. Y. Lin, *J. Am. Chem. Soc.* **2004**, *126*, 13216–13217.
- [21] F. Gao, P. Botella, A. Corma, J. Blesa, L. Dong, *J. Phys. Chem. B* **2009**, *113*, 1796–1804.
- [22] Y. S. Lin, C. P. Tsai, H. Y. Huang, C. T. Kuo, Y. Hung, D. M. Huang, Y. C. Chen, C. Y. Mou, *Chem. Mater.* **2005**, *17*, 4570–4573.
- [23] B. G. Trewyn, S. Giri, I. I. Slowing, V. S. Y. Lin, *Chem. Commun.* **2007**, 3236–3245.
- [24] C. H. Lee, T. S. Lin, C. Y. Mou, *Nano Today* **2009**, *4*, 165–179.
- [25] C. H. Lee, L. W. Lo, C. Y. Mou, C. S. Yang, *Adv. Funct. Mater.* **2008**, *18*, 3283–3292.
- [26] Q. He, Z. Zhang, Y. Gao, J. Shi, Y. Li, *Small* **2009**, *5*, 2722–2729.
- [27] I. Fenoglio, A. Croce, F. Di Renzo, R. Tiozzo, B. Fubini, *Chem. Res. Toxicol.* **2000**, *13*, 489–500.
- [28] A. J. Di Pasqua, K. K. Sharma, Y. L. Shi, B. B. Toms, W. Ouellette, J. C. Dabrowski, T. Asefa, *J. Inorg. Biochem.* **2008**, *102*, 1416–1423.
- [29] Z. Tao, M. P. Morrow, T. Asefa, K. K. Sharma, C. Duncan, A. Anan, H. S. Penefsky, J. Goodisman, A. K. Souid, *Nano Lett.* **2008**, *8*, 1517–1526.
- [30] I. I. Slowing, C. W. Wu, J. L. Vivero-Escoto, V. S. Y. Lin, *Small* **2009**, *5*, 57–62.
- [31] J. D. Bass, D. Grossi, C. Boissiere, E. Belamie, T. Coradin, C. Sanchez, *Chem. Mater.* **2007**, *19*, 4349–4356.
- [32] Q. He, J. Shi, M. Zhu, Y. Chen, F. Chen, *Microporous Mesoporous Mater.* **2010**, *131*, 314–320.
- [33] Q. J. He, J. M. Zhang, J. L. Shi, Z. Y. Zhu, L. X. Zhang, W. B. Bu, L. M. Guo, Y. Chen, *Biomaterials* **2010**, *31*, 1085–1092.
- [34] Y. S. Lin, C. L. Haynes, *J. Am. Chem. Soc.* **2010**, *132*, 4834–4842.
- [35] S. H. Wu, Y. S. Lin, Y. Hung, Y. H. Chou, Y. H. Hsu, C. Chang, C. Y. Mou, *ChemBioChem* **2008**, *9*, 53–57.
- [36] R. Kumar, I. Roy, T. Y. Ohulchansky, L. A. Vathy, E. J. Bergey, M. Sajjad, P. N. Prasad, *ACS Nano* **2010**, *4*, 699–708.
- [37] Y. P. Li, Y. Y. Pei, X. Y. Zhang, Z. H. Gu, Z. H. Zhou, W. F. Yuan, J. J. Zhou, J. H. Zhu, X. J. Gao, *J. Controlled Release* **2001**, *71*, 203–211.
- [38] X. X. He, H. L. Nie, K. M. Wang, W. H. Tan, X. Wu, P. F. Zhang, *Anal. Chem.* **2008**, *80*, 9597–9603.
- [39] Q. J. He, X. Z. Cui, F. M. Cui, L. M. Guo, J. L. Shi, *Microporous Mesoporous Mater.* **2009**, *117*, 609–616.

Received: August 20, 2010

Revised: September 2, 2010

Published online: December 10, 2010

Copyright WILEY-VCH Verlag GmbH & Co. KGaA, 69469 Weinheim, Germany, 2010.



## Supporting Information

for *Small*, DOI: 10.1002/smll.201001459

### **In vivo Biodistribution and Urinary Excretion of Mesoporous Silica Nanoparticles: Effects of Particle Size and PEGylation**

Qianjun He, Zhiwen Zhang, Fang Gao, Yaping Li,\* and Jianlin Shi\*

**In vivo Biodistribution and Urinary Excretion of Mesoporous Silica Nanoparticles:  
 Effects of Particle Size and PEGylation**

*Qianjun He<sup>†</sup>, Zhiwen Zhang<sup>†</sup>, Fang Gao, Yaping Li\*, and Jianlin Shi\**

[\*] Prof. J.L. Shi, Prof. Yaping Li

E-mail: jlshi@sunm.shcnc.ac.cn for J.L. Shi

ypli@mail.shcnc.ac.cn for Y.P. Li

Dr. Q.J. He,<sup>†</sup> Prof. J.L. Shi

State Key Laboratory of High Performance Ceramics and Superfine Microstructure

Shanghai Institute of Ceramics, Chinese Academy of Sciences

1295 Ding-Xi Road, Shanghai 200050 (P. R. China)

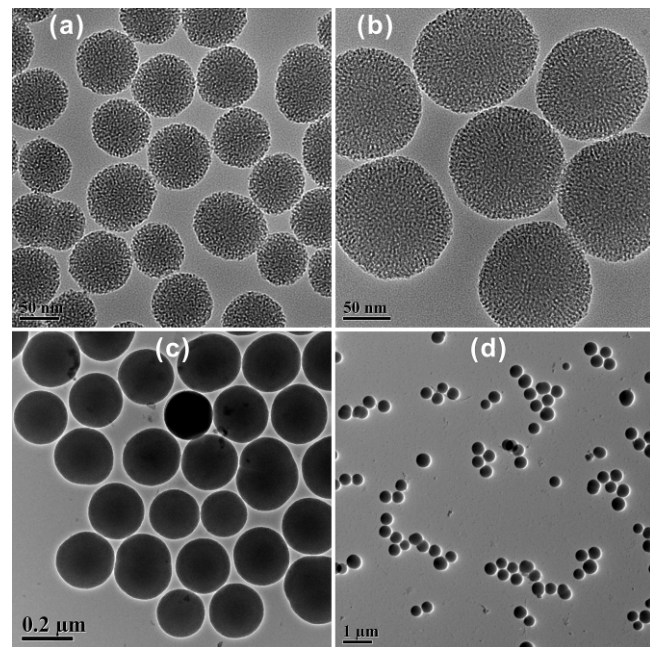
Dr. Z.W. Zhang,<sup>†</sup> Dr. F. Gao, Prof. Y.P. Li

Shanghai Institute of Materia Medica, Chinese Academy of Sciences

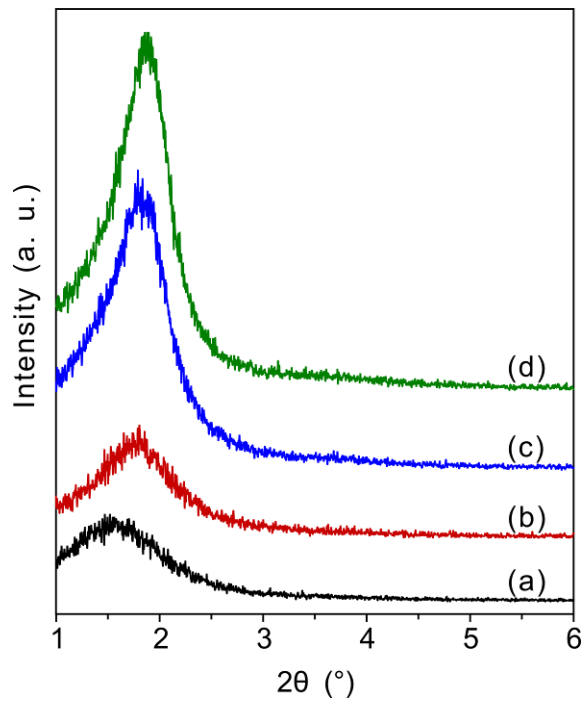
555 Zu Chong-Zhi Road, Shanghai 201203 (P. R. China)

<sup>†</sup> Two authors contributed equally to this work.

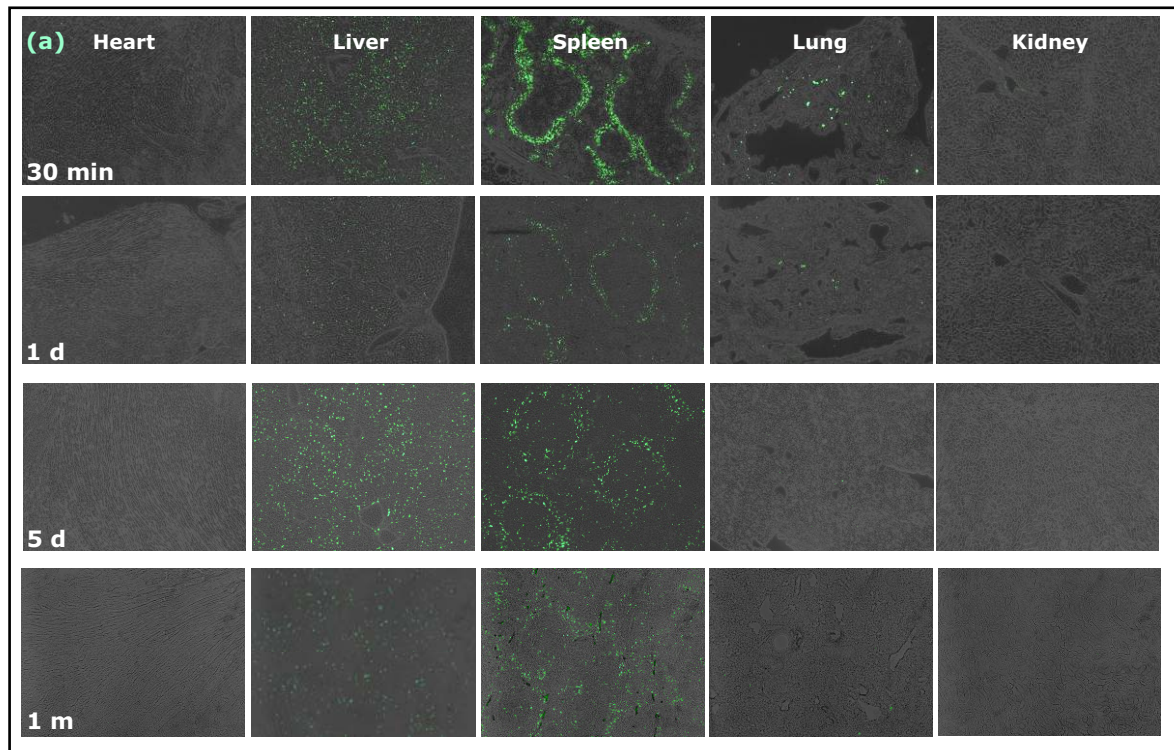
Keywords: biodistribution, excretion, compatibility, mesoporous silica, nanoparticle, PEG

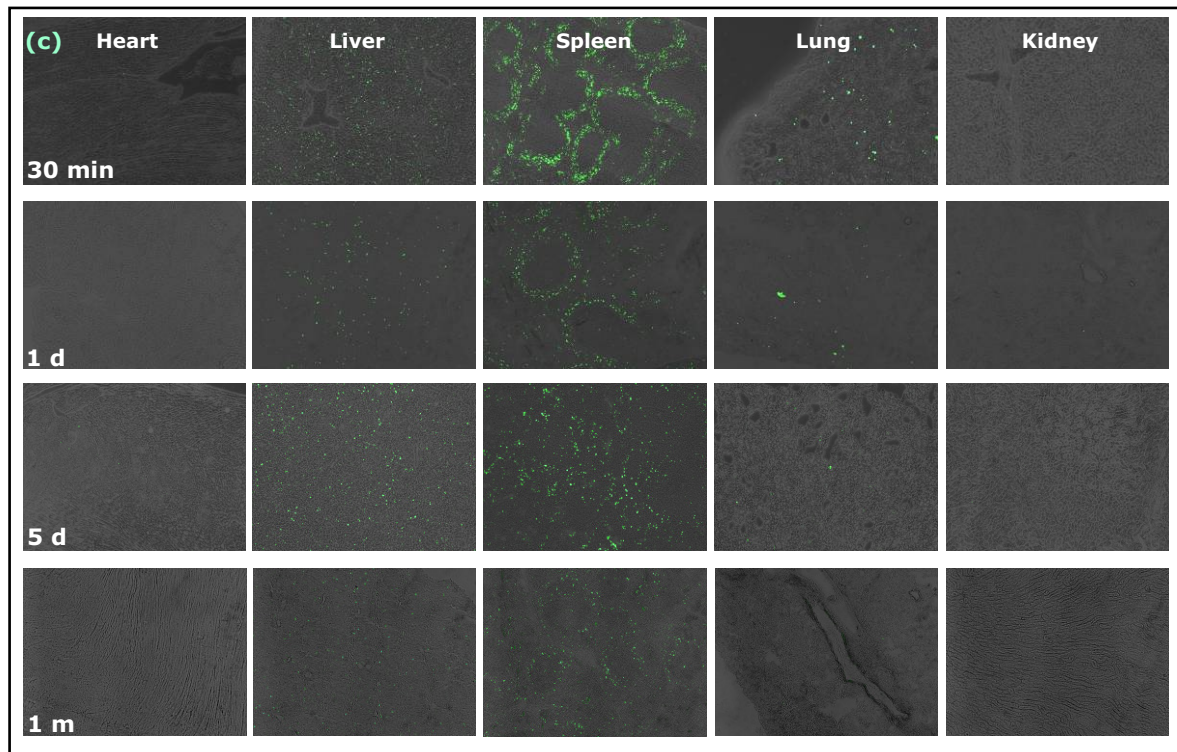
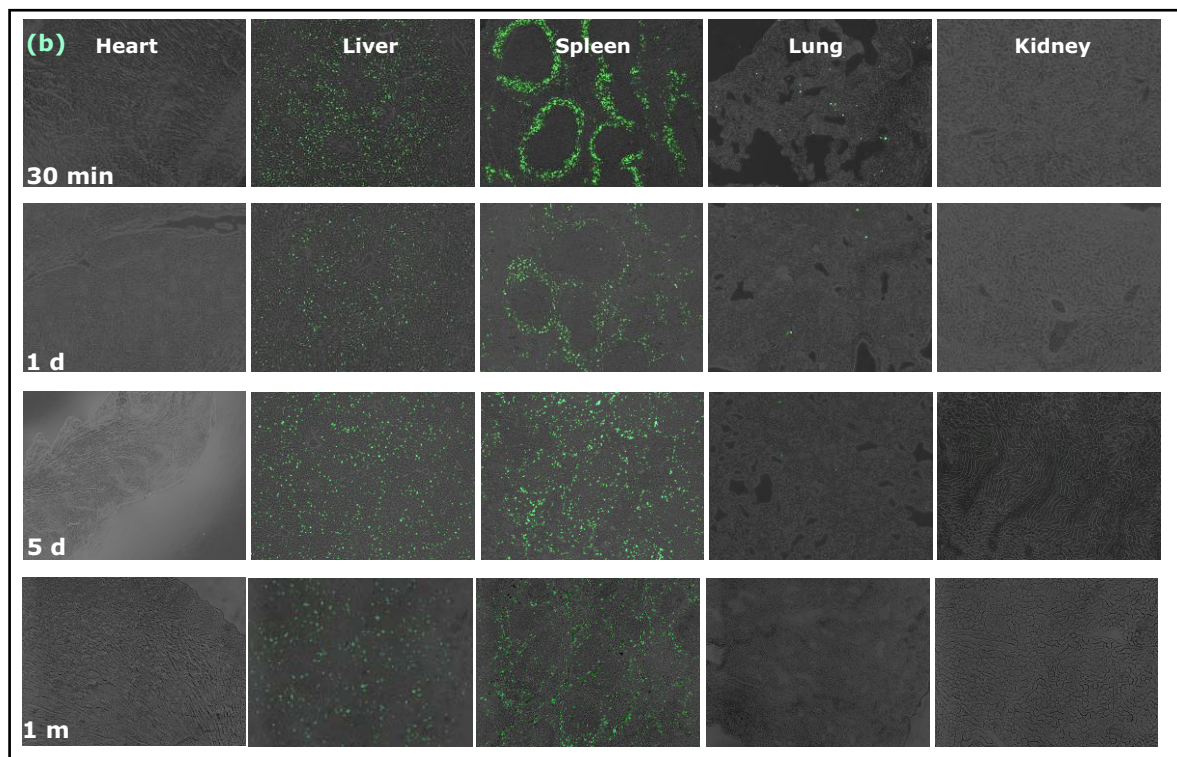


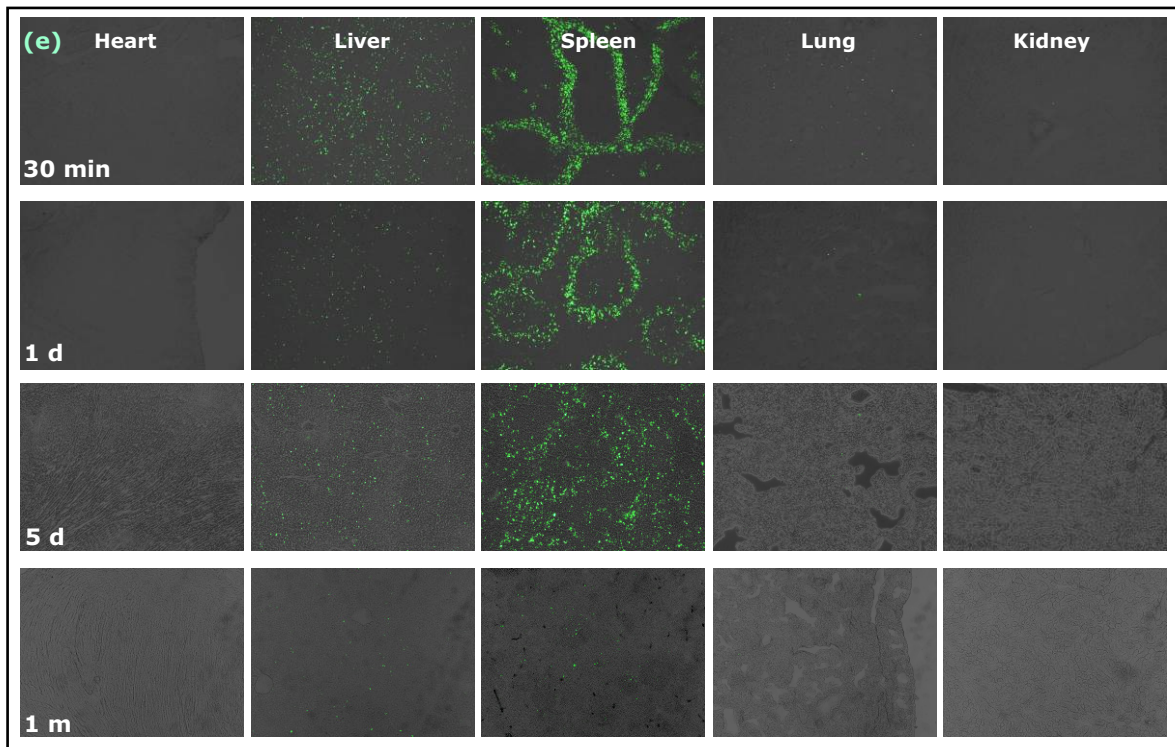
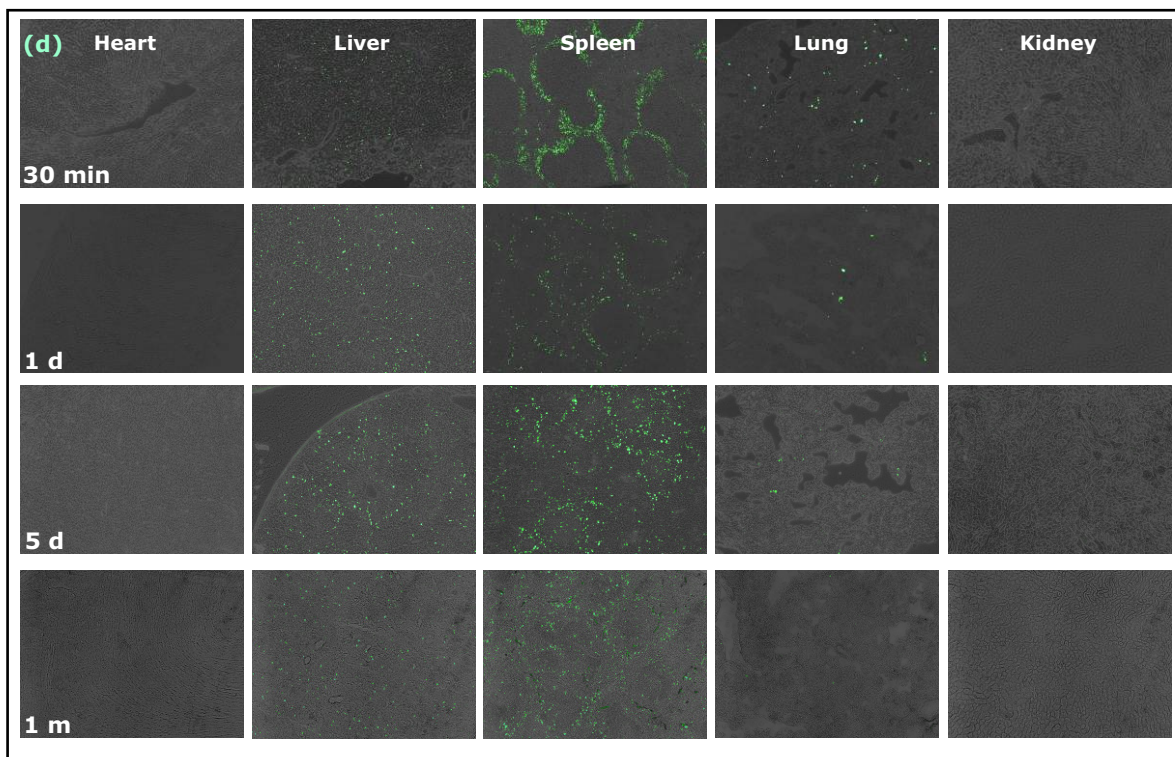
**Figure S1.** TEM images of MSNs of different particle sizes: MSNs-80 (a), MSNs-120 (b), MSNs-200 (c), and MSNs-360 (d). The scale bars of (a), (b), (c) and (d) correspond to 50 nm, 50 nm, 0.2  $\mu$ m and 1  $\mu$ m, respectively.

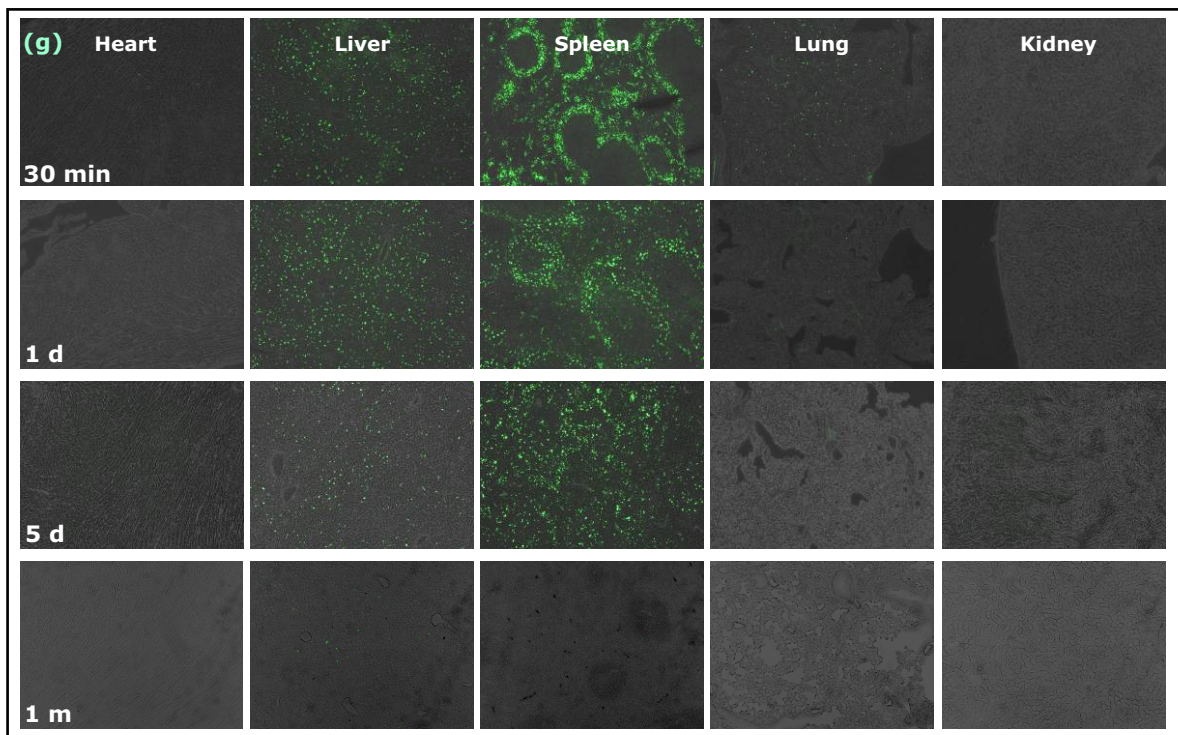
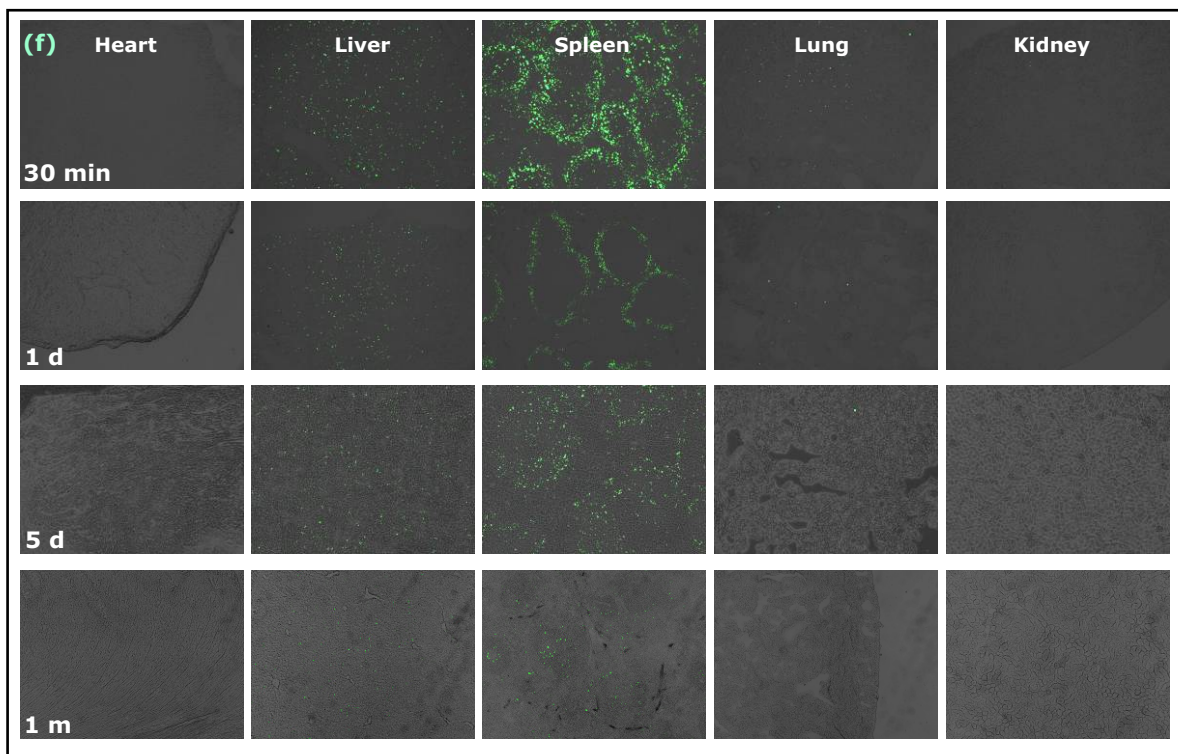


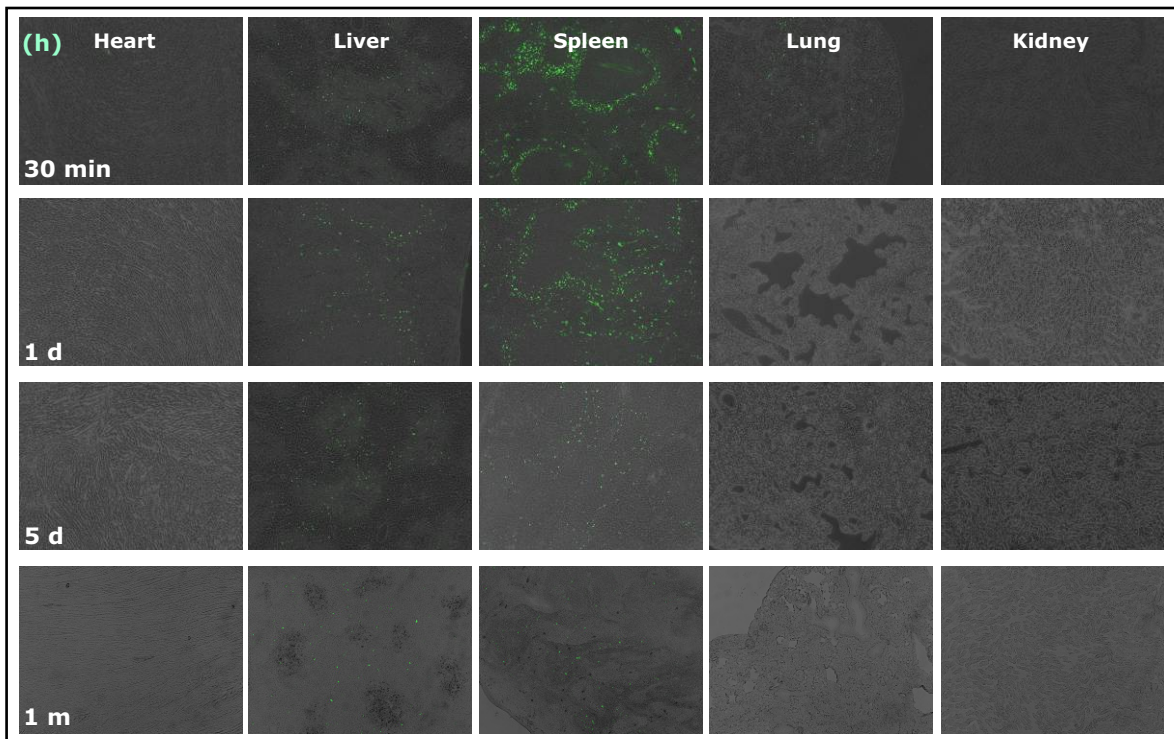
**Figure S2.** SAXRD patterns of MSNs of different particle sizes: MSNs-80 (a), MSNs-120 (b), MSNs-200 (c), and MSNs-360 (d).











**Figure S3.** Fluorescence images of heart, liver, spleen, lung and kidney tissue slices from ICR mice respectively injected with samples MSNs-80 (a), PEG-MSNs-80 (b), MSNs-120 (c), PEG-MSNs-120 (d), MSNs-200 (e), PEG-MSNs-200 (f), MSNs-360 (g) and PEG-MSNs-360 (h) for different time periods (30 min, 1 d, 5 d and 1 m).